Ulster
University

Development of a first-in-class unimolecular dual GIP/GLP-2 analogue, GL-0001, for the treatment of bone fragility

Link to publication record in Ulster University Research Portal

Document Version
Publisher's PDF, also known as Version of record

RESEARCH ARTICLE

Development of a First-in-Class Unimolecular Dual GIP/GLP-2 Analogue, GL-0001, for the Treatment of Bone Fragility

Benoit Gobron,[1,2] Malory Couchot,[1,3] Nigel Irwin,[4] Erick Legrand,[1,2] Béatrice Bouvard,[1,2] and Guillaume Mabilleau[1,5]

[1]Univ Angers, Nantes Université, ONIRIS, Inserm, RMeS, UMR 1229, SFR ICAT, Angers, France
[2]CHU Angers, Service de Rhumatologie, Angers, France
[3]SATT Ouest Valorisation, Nantes, France
[4]Ulster University, School of Pharmacy and Pharmaceutical Sciences, Coleraine, UK
[5]CHU Angers, Departement de Pathologie Cellulaire et Tissulaire, UF de Pathologie osseuse, Angers, France

ABSTRACT

Due to aging of the population, bone frailty is dramatically increasing worldwide. Although some therapeutic options exist, they do not fully protect or prevent against the occurrence of new fractures. All current drugs approved for the treatment of bone fragility target bone mass. However, bone resistance to fracture is not solely due to bone mass but relies also on bone extracellular matrix (ECM) material properties, i.e., the quality of the bone matrix component. Here, we introduce the first-in-class unimolecular dual glucose-dependent insulinotropic polypeptide/glucagon-like peptide-2 (GIP/GLP-2) analogue, GL-0001, that activates simultaneously the glucose-dependent insulinotropic polypeptide receptor (GIPr) and the glucagon-like peptide-2 receptor (GLP-2r). GL-0001 acts synergistically through a cyclic adenosine monophosphate-lysyl oxidase pathway to enhance collagen maturity. Furthermore, bilateral ovariectomy was performed in 32 BALB/c mice at 12 weeks of age prior to random allocation to either saline, dual GIP/GLP-2 analogues (GL-0001 or GL-0007) or zoledronic acid groups ($n = 8$/group). Treatment with dual GIP/GLP-2 analogues was initiated 4 weeks later for 8 weeks. At the organ level, GL-0001 modified biomechanical parameters by increasing ultimate load, post-yield displacement, and energy-to-fracture of cortical bone. GL-0001 also prevented excess trabecular bone degradation at the appendicular skeleton and enhanced bone ECM material properties in cortical bone through a reduction of the mineral-to-matrix ratio and augmentation in enzymatic collagen cross-linking. These results demonstrate that targeting bone ECM material properties is a viable option to enhance bone strength and opens an innovative pathway for the treatment of patients suffering from bone fragility. © 2023 The Authors. *Journal of Bone and Mineral Research* published by Wiley Periodicals LLC on behalf of American Society for Bone and Mineral Research (ASBMR).

KEY WORDS: UNIMOLECULAR DUAL GIP/GLP-2 ANALOGUE; BONE MATERIAL PROPERTIES; BONE FRAGILITY

Introduction

Due to aging of the population, the occurrence of bone fragility and fracture has risen significantly worldwide and will continue to rise in the future.[1] Bone fragility develops as a concomitant decline in bone mass and bone quality. Bone mass is regulated by a complex balance between catabolic removal of quanta of bone material by osteoclasts and anabolic deposition of quanta of bone material by osteoblasts. All Food and Drug Administration (FDA)-approved drugs for the treatment of osteoporosis and bone fragility are based on either limiting osteoclast-mediated bone resorption or enhancing osteoblast-mediated bone formation. Strontium ranelate, approved in Europe for the treatment of severe osteoporosis, acts differently through a purely physicochemical mechanism, thereby promoting osteoblast function and inhibiting osteoclast function.[2] This is based on the idea that increasing bone mineral density, the clinical surrogate for bone mass assessment, will result in higher

bone strength. Although this is partly true in osteoporosis, and despite the fact that all approved anti-osteoporotic drugs increase bone mineral density, the risk of bone fracture is only reduced by 30%–40% in hip and long bones in treated individuals.[3-6] This suggests that factors beyond bone mass are primordial for optimum bone strength.

Bone quality is also compromised in bone fragility.[7] Bone quality encompasses an ensemble of factors, including bone microstructure, bone extracellular matrix (ECM) material properties, and resistance to crack propagation.[8] Indeed, despite the relatively simple structure of the collagen triple helix, the biosynthesis of collagen molecules by osteoblasts undergoes multiple posttranslational steps to ensure proper folding and resistance to deformation. Among all, enzymatic collagen cross-linking, ensured by lysyl hydroxylase and lysyl oxidase (LOX), has attracted attention.[9] To date, only a few signaling pathways known to regulate bone ECM material properties have been identified.[10-13] Unraveling the mechanisms controlling bone ECM material properties should lead to the development of bone quality-specific drugs that could represent an interesting alternative to existing medications.

The idea of selectively targeting bone ECM material properties to improve bone strength, rather than directly addressing low bone mass, has emerged as a result of pioneering works with two endogenous gut hormones, glucose-dependent insulinotropic polypeptide (GIP) and glucagon-like peptide-2 (GLP-2). Indeed, these peptides maintain optimal bone ECM material properties through a cyclic adenosine monophosphate (cAMP)-dependent pathway.[14-17] This concept was also reinforced by the use of first-generation GIPr- and GLP-2r-specific analogues in several mice models of bone fragility.[18-22] Furthermore, head-to-head comparison in preclinical model of bone fragility suggested that single GIP or GLP-2 analogues exhibited similar bending strength and postyield deformation, as observed with bisphosphonates in the appendicular skeleton.[18,23] However, this effect was not observed with the closely related glucagon or GLP-1 peptides, highlighting the selective bone response to GIP and GLP-2 single analogues. This is particularly interesting with respect to the recent evidence that functional GIPr and GLP-2r are also present in human bone cells.[24,25]

Recently, it was reported that GIP and GLP-2 exert separate beneficial effects on bone turnover represented by GIP-independent suppression of bone resorption by GLP-2 and significant increases in bone formation by GIP.[26] GIP or GLP-2 single analogues were also able to enhance collagen postprocessing and maturity in vitro and in vivo.[15-18] Furthermore, a higher mineral-to-matrix ratio has also been reported in ovariectomized mice, and administration of GLP-2 single analogue was capable of reducing this parameter to levels observed in sham animals.[18] Based on these outcomes, and in light of improvements in collagen maturity observed with both single GIP and GLP-2 analogues and restoration of the mineral-to-matrix ratio with the GLP-2 single analogue, we hypothesized that coadministration of single GIP or GLP-2 analogues would result in synergistic effects compared with single parent molecules and would surpass the beneficial effects of bisphosphonates on bone resistance to fracture. Here, to overcome possible discrepancies in the pharmacokinetic profiles of GIP and GLP-2 analogues, we developed a series of unimolecular dual GIP/GLP-2 analogues and tested their capacity to bind and activate the human GIPr and GLP-2r, while also evaluating their capacity to enhance bone ECM material properties. Finally, we identified our lead molecule, a first-in-class unimolecular dual GIP/GLP-2 analogue, GL-0001. The latter dually binds the GIPr and GLP-2r and activates intracellular production of cAMP, resulting in a higher expression of Lox and, ultimately, higher collagen cross-linking. GL-0001-mediated changes in bone ECM material properties also improved bone strength in an approved mouse model of ovariectomy (OVX)-induced bone fragility. Unimolecular dual GIP/GLP-2 analogues represent an innovative and novel pathway to treat bone fragility that should be further explored for the treatment of bone fragility disorder.

Material and Methods

A table of key resources is supplied as Table S1.

Osteoblast cultures

Murine MC3T3-E1 cells were grown in α modified essential medium (αMEM) supplemented with 10% fetal bovine serum (FBS), 100 UI/mL penicillin, and 100 μg/mL streptomycin in a humidified atmosphere enriched with 5% CO_2 at 37°C. For differentiation studies, cells were plated at a density of 15,000 cells/cm^2, grown to confluence and differentiated in medium supplemented with 50 μg/mL ascorbic acid and several concentrations of peptides. Fourteen days later, osteoblast cultures were fixed in absolute ethanol, scrapped off the culture dish and transferred onto BaF2 windows for evaluation of collagen maturity, or prepared for gene expression.

For mechanistic investigations, administration of 50 μM 2′, 5′ dideoxyadenosine (2′, 5′-DDA)[16] and 0.25 mM beta-aminopropionitrile (bAPN)[27] were added in the differentiation medium and replenished every other day. For silencing experiments, at day 7 of the differentiation studies, osteoblasts were transfected with 50 nM of small interfering ribonucleic acid (siRNA) targeting murine GIPr (assay ID s233873), murine GLP-2r (assay ID s211996), murine LOX (assay ID s69290), or a control scrambled siRNA (ref 4390843) using lipofectamine RNAimax. Experiments were terminated at day 14, and ECM properties were evaluated as stated in what follows.

Normal human osteoblasts were plated at a density of 5,000 cells/cm^2 in Clonetics™ OGM™ osteoblast growth medium. At 80% confluence, 200 nM hydrocortisone-21-hemissucinate was added to the culture to induce differentiation. Ninety-five days later, osteoblast cultures were fixed and processed as described earlier for murine osteoblasts.

Intracellular cAMP determination in osteoblast cultures

MC3T3-E1 cells were plated at a density of 15,000 cells/cm^2 and grown for 48 hours in αMEM supplemented with 10% FBS, 100 UI/mL penicillin, and 100 μg/mL streptomycin in a humidified atmosphere enriched with 5% CO_2 at 37°C. After 48 hours, cells were starved in αMEM supplemented with 0.5% bovine serum albumin (BSA) for 16 hours and then incubated for 15 minutes in αMEM supplemented with 0.5% BSA and 1 mM 3-isobutyl-1-methylxanthine prior to stimulation with peptides. After 45 minutes, cells were washed with ice-cold phosphate buffer saline (PBS), incubated in radioimmunoprecipitation assay buffer, and centrifuged at 13,000 g for 10 minutes. Supernatants were collected and stored at −80°C until use. cAMP determination was performed with a commercially available enzyme immunoassay (EIA) kit according to the manufacturer's recommendations.

Binding assay and receptor activation

Human GIPr and human GLP-2r cDNAs were cloned in pcDNA3.1 between XhoI and AgeI of the multiple cloning sites. For binding assay, CHO-K1 cells were transfected with pcDNA3.1(hGIPr) or pcDNA3.1(hGLP-2r) using Lipofectamine™ 3000. Forty-eight hours later, various concentrations of analogues were added in the presence of either 10^{-7} M Fam-[D-Ala^2]-GIP$_{1-30}$ or 10^{-6} M Fam-[Gly^2]-GLP-2 in αMEM supplemented with 0.1% BSA. These concentrations of fluorescent peptides were determined on preliminary assays and represented 100% binding. Equilibrium binding was achieved overnight at 4°C. Cells were then washed twice with assay buffer and solubilized in 0.1 M NaOH. Fluorescence was read with a SpectraMax M2 microplate reader with excitation wavelength set up at 490 nm and emission wavelength set up at 525 nm. Binding at the human GIP receptor or human GLP-2 receptor was achieved by nonlinear regression analysis.

For activation assay, plasmids encoding the human GIPr, human GLP-2r, and Epac-S-H74 probe, a validated cAMP Förster resonance energy transfer (FRET) biosensor,[28] were transfected with Lipofectamine™ 3000 into CHO-K1 cells. Forty-eight hours later, transfected cells were incubated in HEPES buffered saline in the presence of various concentrations of peptides for 30 minutes. Donor excitation was made at 460 nm, donor emission was collected at 480 nm, and acceptor emission was collected at 560 nm with an M2 microplate reader. FRET was expressed as the ratio between donor and acceptor signals. The FRET ratio was standardized at 1 with vehicle. An increase in the FRET ratio suggests an augmentation in intracellular cAMP levels.

Gene expression

For osteoblast cultures, total RNA was extracted after rinsing cultures with PBS. Ex vivo gene expression analysis was performed after crushing left tibia in a liquid nitrogen-cooled biopulverizer. Nucleozol (Macherey-Nagel, Hoerdt, France) was added on top of the cell layer/bone powder, and total RNA were purified with Nucleospin RNA set nucleozol column (Macherey-Nagel) according to the manufacturer's recommendations. Total RNA was reverse-transcribed using Maxima first strand cDNA synthesis kit. Real-time qPCR was performed using TaqMan™ Fast advanced master mix and TaqMan Gene Expression Assays for *Lox* (Mm00495386_m1), *Col1a1* (Mm00801666_g1), *Alpl* (Mm00475834_m1), and *Plod2* (Mm00478767_m1). The *B2m* endogenous control (Mm00437762_m1) was used for normalization using the $2^{-\Delta\Delta CT}$ method.

Osteoclast cultures

Murine Raw 264.7 cells were plated at a concentration of 125,000 cells/cm^2 in osteoclast medium containing αMEM supplemented with 10% FBS, 2 mM L-glutamine, 100 U/ml penicillin, and 100 μg/ml streptomycin. To generate osteoclasts from Raw 264.7 cells, osteoclast medium was enriched with 25 ng/ml soluble receptor activator of nuclear factor κB ligand (sRANKL), and several concentrations of peptides were then added to test their effects on osteoclast differentiation. After 5 days of culture, cytochemical tartrate-resistant acid phosphatase (TRAcP) staining was performed to reveal the presence of osteoclast cells (TRAcP positive [TRAcP$^+$] cells with more than three nuclei).

Isolated human peripheral blood mononuclear cells were plated at a concentration of 100,000 cells/cm^2 in osteoclast medium enriched with 25 ng/ml recombinant human macrophage colony-stimulating factor, 25 ng/ml recombinant human sRANKL (added at day 7), and various concentrations (10^{-10} to 10^{-8} M) of peptides (added at day 7). Cultures made for the assessment of osteoclast resorption were plated on collagen-coated plastic plates. Cultures were terminated after 14 days to assess the extent of osteoclast formation (TRAcP$^+$ cells with more than three nuclei) or at 21 days to assess the extent of osteoclast resorption (see following discussion). All factors were replenished every 2–3 days.

The expression of TRAcP was examined cytochemically, as described previously,[29] using naphthol AS-BI-phosphate as substrate and fast violet B as the diazonium salt. Cells were counterstained with 4, 6-diamidino-2-phenylindole (DAPI).

For the assessment of osteoclast resorption, human osteoclasts cultured on collagen-coated plates were incubated with collagenase at day 20. The cell suspension was passed through a cell strainer with 40-μm pores, and the fraction retained in the strainer was plated on dentine slices at a concentration of 5,000 cells/cm^2 and cultured for an additional 24 hours. After discarding osteoclasts, dentine slices were stained with 0.5% (v/v) toluidine blue (pH 5.0) prior to examination by light microscopy for the presence of lacunar resorption, and the extent of surface erosion on dentine slices was determined using image analysis as described previously.[30]

Animals

All procedures were carried out in accordance with the European Union Directive 2010/63/EU for animal experiments and were approved by the regional ethics committee for animal use (authorization CEEA-PdL06-01740.01). Briefly, bilateral OVX was performed in 32 BALB/c (BALB/cJRj) mice at 12 weeks of age under general anesthesia. At 16 weeks of age, osmotic minipumps were implanted subcutaneously between the two scapulae in 24 ovariectomized mice that were randomly allocated into either saline (OVX + saline, $n = 8$), 25 nmoles/kg/day GL-0001 (OVX + GL-0001, $n = 8$), or 25 nmoles/kg/day GL-0007 (OVX + GL-0007, $n = 8$). These doses of unimolecular dual GIP/GLP-2 analogues were based on previous studies performed with single-parent peptides.[18,23] Eight ovariectomized BALB/c mice received an intravenous injection of zoledronic acid (100 μg/ kg) and were implanted subcutaneously with an osmotic minipump filled with saline at 16 weeks of age (OVX + Zoledronic acid). Eight sham operated female BALB/c mice of the same age and implanted with osmotic minipumps delivering saline were used as negative controls (sham+saline). Treatment with saline or dual GIP/GLP-2 analogues lasted for 8 weeks. Osmotic minipumps were exchanged after 4 weeks. All animals received an intraperitoneal administration of calcein green (10 mg/kg) 10 days and 2 days before sacrifice. Fig. S1 presents a schematic of the animal study. Animals were housed in social groups and maintained in a 12 hours:12 hours light:dark cycle and had free access to water and diet. No adverse events were observed in any of the group. At necropsy, blood collection by intracardiac aspiration (~250 μl) was performed in EDTA-treated tubes. Blood samples were spun at 13,000*g* for 15 minutes, aliquoted, and stored at −80°C until measurement of plasma level of CTX-I and P1NP. Uteruses were collected and weighed to ensure optimum OVX. Right and left hindlimbs, as well as fourth lumbar vertebrae, were collected and cleaned of soft tissue. Right femurs and fourth lumbar vertebrae were wrapped in saline-soaked gauze and frozen at −20°C until use. Left tibias were snap frozen

in RNA later and stored at −80°C until use. Other bones were stored in 70% ethanol.

High-resolution X-ray micro–computed tomography

Micro–computed tomography (μCT) analyses were performed at the right tibia, right femur, and fourth lumbar vertebrae with a Bruker 1272 microtomograph operated at 70 kV, 140 μA, 1000 ms integration time, and imaging in water. The isotropic pixel size was fixed at 4 μm and the rotation step at 0.25°, and exposure was performed with a 0.5-mm aluminum filter. Hydroxyapatite phantoms (250 mg/cm^3 and 750 mg/cm^3) were used for calibration. Reconstruction of 2D projections was done using NRecon software (version 1.6.10.2). For tibial analysis, a trabecular volume of interest was located 0.5 mm below the growth plate at the proximal end and extended 2 mm down. The fourth lumbar vertebra was used as a second site rich with trabecular bone. The vertebral trabecular region of interest was represented by the vertebral body. Trabecular bone was separated from cortical bone with an automatic contouring script in CTan software (version 1.20.8.0). The right femur was used for cortical microarchitecture. The region analyzed (0.5 mm) was centered at the midpoint between the third trochanter and the distal growth plate. Bone was segmented from soft tissue using global thresholding set at 300 mg/cm^3 for trabecular bone and 700 mg/cm^3 for cortical bone. All histomorphometrical parameters were measured with the CTan software according to guidelines and nomenclature proposed by the American Society for Bone and Mineral Research.[31]

Bone histomorphometry

After μCT scans, right tibias were embedded undecalcified in polymethylmethacrylate (pMMA) at 4°C. For each animal, four nonserial longitudinal sections (∼50 μm apart) were counterstained with calcein blue for dynamic histomorphometry, and four additional sections were stained for TRAcP, as previously described.[32] The histomorphometrical parameters of bone formation were computed using CalceinHisto software developed by Professor Rob van't Hof (Institute of Aging and Chronic Disease, University of Liverpool, UK).[33] Standard bone histomorphometrical nomenclatures, symbols, and units were used as described in the guidelines of the American Society for Bone and Mineral Research.[34] The identity of the sections was not revealed to the pathologist until the end of all measurements.

Assessment of bone strength

The whole-bone strength of the right femurs was assessed by three-point bending, as described previously,[17,35] and in accordance with published guidelines.[36] Three-point bending strength was measured with a constant span length of 10 mm. Bones were tested in the anteroposterior axis with the posterior surface facing upward, centered on the support, and the pressing force was applied vertically to the midshaft of the bone. A compression test was performed on the vertebral body of the fourth lumbar vertebra in the craniocaudal direction. Briefly, the caudal surface was placed on a lab-made device consisting of a platen and a metal pin (800 μm diameter) inserted into the vertebral canal. A 5-mm-diameter puncture probe was used to apply compression on the cranial surface of the vertebra. Each bone was tested fully hydrated and at room temperature and a loading speed of 2 mm.min^{-1} until failure with a 500-N load cell on an Instron 5942 device (Instron, Elancourt, France), and the load–displacement curve was recorded at a rate of 100 Hz using Bluehill 3 software (Instron). Ultimate load, ultimate displacement, stiffness, and work to fracture were calculated as indicated in Turner and Burr.[37] The yield load was determined as the point at which a regression line that represents a 10% loss in stiffness crossed the load–displacement curve. Postyield displacement was computed as the displacement between yielding and fracture.

Bone ECM material evaluation

For collagen cross-link analysis in osteoblast cultures, the ECM was prepared as already reported.[16] Spectral analysis was performed using a Bruker Hyperion 3000 infrared microscope coupled to a Bruker Vertex 70 spectrometer and standard single-element mercury cadmium telluride detector. Mid-infrared spectra were recorded at a resolution of 4 cm^{-1} (spectral range 750–2000 cm^{-1}), with 128 accumulations in transmission mode. For the analysis of bone specimen, left femurs were embedded undecalcified in pMMA after dehydration and infiltration as previously reported.[17] A 1-μm-thick cross section of the midshaft femur was cut with an ultramicrotome (Leica EM UC7, Leica microsystems, Nanterre, France) and deposited on BaF2 windows. Spectral analysis was performed with the same setup (Bruker Hyperion 3000 infrared microscope/Vertex 70 spectrometer) using a 64 × 64 focal plane array detector. A field of view of 540 × 540 μm covering the posterior quadrant of the femur midshaft was analyzed. Mid-infrared spectra were recorded at a resolution of 8 cm^{-1} (spectral region 900–2000 cm^{-1}), with 32 accumulations in transmission mode.

For extracellular matrix and femur cross section, background spectra were collected under identical conditions from the same BaF$_2$ windows at the beginning and end of each experiment to ensure instrument stability. Postprocessing was performed using MATLAB R2021b (MathWorks, Natick, MA) and included Mie scattering correction, pMMA subtraction (femur cross section only), normalization, denoising (Savitzky–Golay algorithm, degree 2, span 9) prior to second derivative spectroscopy, and curve-fitting routines as previously reported.[38] A signal-to-noise ratio was computed in the 1850–2000 cm^{-1} region to ensure proper denoising and quality of Fourier transform infrared (FTIR) spectra. Figures S2 and S3 provide a schematic of the experimental procedures used for ECM assessment in osteoblast cultures and bone samples.

The ECM material parameter analyzed for osteoblast cultures was collagen maturity (area ratio 1660/1690 cm^{-1}). Combination indices were computed according to Chou and Talalay's method[39] assuming a bliss independence model as

$$CI = \frac{[E_{GIP} + E_{GLP-2} - (E_{GIP} * E_{GLP-2})]}{E_{DA}}$$

where E_{GIP}, E_{GLP-2}, and E_{DA} represent the effects on collagen maturity observed with GIP alone, GLP-2 alone, or unimolecular dual GIP/GLP-2 analogue, respectively, as compared with vehicle-treated cultures.

Bone ECM material parameters for cortical cross section were as follows: mineral-to-matrix ratio (area of v1, v3 phosphate/area amide I); mineral crystallinity/maturity (intensity ratio 1030 cm^{-1}/1020 cm^{-1}); carbonate/phosphate ratio (intensity v3 carbonate located at ∼1415 cm^{-1}/1030 cm^{-1}); trivalent collagen cross-link content (intensity 1660 cm^{-1}/area Amide I);

divalent collagen cross-link content (intensity 1690 cm^{-1}/area Amide I); and collagen maturity (intensity ratio 1660 cm^{-1}/1690 cm^{-1}).[40] Histogram distribution for each compositional parameter was fitted with a Gaussian model and considered normal if the R^2 coefficient was >0.95. In the present study, no histogram deviated from a normal distribution. For each of the compositional parameters, the mean of the pixel distribution (excluding nonbone pixels) was computed as

$$\text{Mean} = \frac{\sum (Xi \times Fi)}{N}$$

where Xi represents the value of the FTIR parameter for the ith bin, Fi is the percentage of bone area with the Xi value, and N is the total number of bins in the histogram distribution.

GL-0001 degradation

Fifty micrograms of PYY$_{1-36}$ or GL-0001$_{1-33}$ were incubated at 37°C on a plate shaker in 50 mM triethanolamine/HCl (pH 7.8) with 0.05 U of pure DPP-4 enzyme for 0, 0.5, 1, 2, and 8 hours. Reactions were terminated, as appropriate, via the addition of 10% (v/v) trifluoroacetic acid/water. Reaction mixes were separated by reverse-phase high-performance liquid chromatography (RP-HPLC) with absorbance monitored at 214 nm using a Thermo Separation SpectraSYSTEM UV2000 detector. HPLC peaks were collected and identified via MALDI-ToF MS on a PerSeptive Biosystems Voyager-DE Biospectrometry (Hertfordshire, UK). Percentages of intact and cleaved peptides were computed based on the area of the corresponding peak on the HPLC profiles.

Statistical analysis

The sample size for the mouse experiments was estimated based on previous experiments in our laboratory[18,23] using energy-to-fracture as a primary outcome. Secondary outcomes of interest included effects on collagen maturity and trabecular bone mass. Statistical analyses were performed with GraphPad Prism 8.0 (GraphPad Software, La Jolla, CA, USA). The Brown-Forsythe test of equal variance was applied, and when normality was respected, ordinary one-way ANOVA with multiple post hoc Dunnett comparisons were conducted. When normality was not respected, Kruskal-Wallis tests with multiple post hoc Dunn's comparisons were carried out. Linear regression was computed to correlate biomechanical properties with bone turnover, bone structure, and bone ECM material properties. Mixed model analysis was conducted to assess changes in body weights with Dunnett's multiple comparison test. Unless otherwise stated, data are presented as boxplots with median and interquartile range (25th to 75th percentiles). Differences at $p < 0.05$ were considered significant.

Results

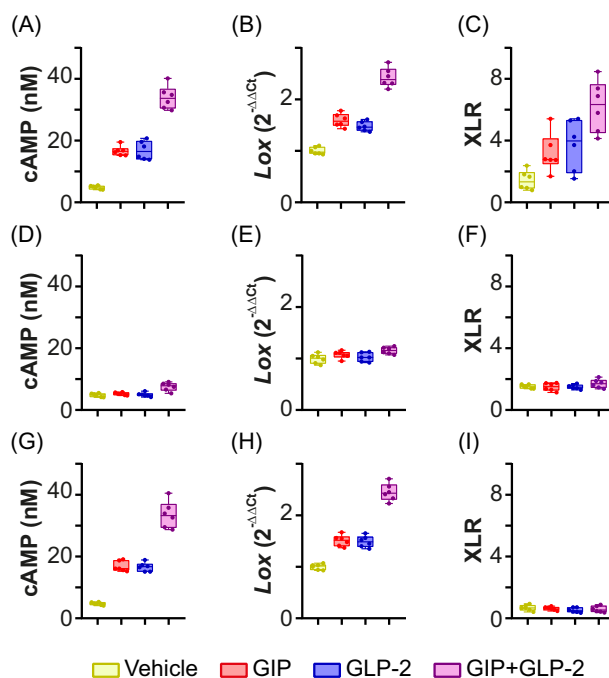### Coadministration of GIP and GLP-2 agonists modulated bone ECM material properties

As a proof of concept, and to follow our previous work on first-generation analogues,[15,16] we coadministered the GIP and GLP-2 analogues, [D-Ala^2]GIP$_{1-30}$ and [Gly^2]GLP-2, in murine MC3T3-E1 osteoblast cultures at a concentration of 100 pM. This

concentration was previously found to exhibit a pronounced biological response.[15] As compared with vehicle or with single agonist, coadministration resulted in higher levels of intracellular cAMP (Fig. 1A). The same pattern was also observed for the expression of *Lox*, a key enzyme involved in enzymatic collagen cross-linking (Fig. 1B), and ultimately led to higher levels of collagen cross-linking (Fig. 1C). These effects were drastically reduced if osteoblasts had been previously treated with 2′, 5′-dideoxyadenosine, a selective adenylyl cyclase inhibitor (Fig. 1D–F), suggesting that enhanced expression of *Lox* and collagen cross-linking in response to single agonists or coadministration is cAMP-dependent. The use of bAPN, a selective lysyl oxidase inhibitor that acts by binding irreversibly to the lysyl oxidase binding site,[27] hampered the response observed with GIP or GLP-2 single agonists and with coadministration (Fig. 1G–I). Together these data supported our initial hypothesis that coadministration of GIP and GLP-2 analogues exert additive effects and enhance collagen postprocessing to a higher extent, as seen with single-parent peptides, and hence may improve bone ECM material properties through a cAMP-lysyl oxidase pathway.

Development and validation of a series of unimolecular dual GIP/GLP-2 analogues

We then performed a sequence alignment between human GIP and human GLP-2. Since the first 30 amino acids of human GIP and GLP-2 are sufficient to induce biological activity,[41,42] we only used this portion for sequence alignment. Human GIP and GLP-2 share ~67% similarity with divergence at positions 7, 12, 13, 18, 19, 28, and 29. The observed similarity and divergence at key positions was used as the basis for developing a new class of synthetic molecules, namely unimolecular GIP/GLP-2 dual analogues. Optimization of the consensus sequence was performed in silico based on available information regarding the structure–activity relationship and published docking studies between human GIP or GLP-2 and their respective receptors.[42-48] The dipeptidyl peptidase-4 (DPP-4) is known to cleave GIP and GLP-2 between the second and third amino acids, leading to inactive peptides.[49] To confer resistance to DPP-4 degradation, a glycine residue was introduced at position 2 of unimolecular dual GIP/GLP-2 analogues. We synthesized nine different unimolecular dual GIP/GLP-2 analogues, called GL-000x with x ranging between 1 and 9, and further investigated their biological potency in vitro.

Because binding, but more importantly activation, of cAMP appeared crucial in coadministration studies, we set out to determine whether unimolecular dual GIP/GLP-2 analogues could bind to both the human GIPr and human GLP-2r and activate the production of cAMP (Table 1). Interestingly, in our competition assay, most dual GIP/GLP-2 analogues bound to the human GIPr with affinity, as represented by IC$_{50}$, similar to GIP$_{1-30}$ at the exception of GL-0005, GL-0006, and GL-0009. However, only GL-0001, GL-0007, and GL-0008 significantly raised intracellular levels of cAMP, represented by a higher FRET ratio, suggesting binding to and activation of the human GIPr. At the human GLP-2r, GL-0001, GL-0004, GL-0007, and GL-0008 presented with similar binding affinity compared with human GLP-2. Interestingly, GL-0001, GL-0004, and GL-0007 led to higher intracellular levels of cAMP, suggesting here again that these molecules not only bind to but also activate human GLP-2r. We also computed changes in the FRET ratio compared with the conventional ligand at both receptors. These data were used to compute a coagonism score to appreciate the activity at both receptors

Fig. 1. Coadministration of GIP and GLP-2 single analogues enhanced collagen maturity through a cAMP-lysyl oxidase pathway. Murine MC3T3-E1 osteoblasts were treated with vehicle, 100 pM [D-Ala^2]GIP$_{1-30}$, 100 pM [Gly^2]GLP-2, or coadministration of both analogues. (A, D, G) cAMP levels were determined 48 hours after treatment by EIA. (B, E, H) *Lox* expression and (C, F, I) collagen maturity (XLR) were determined after 14 days of treatment with the aforementioned peptides. To elucidate the molecular pathway involved in enhanced collagen maturity, MC3T3-E1 cells were treated with either DDA (D–F) or bAPN (G–I). Statistical analyses were performed with Kruskal-Wallis with Dunn's post hoc test. Data are presented as boxplot showing 25th and 75th percentiles, with whiskers, showing minimal and maximal values.

(Table 1). Theoretically, a score above 0.5 suggests coagonism. These data suggest that GL-0008 and GL-0004 are single agonists of human GIPr and human GLP-2r, respectively. Interestingly, these data also support a coagonism action of GL-0001 and GL-0007.

Evaluation of biological activity of unimolecular dual GIP/GLP-2 analogues

Because higher expression of *Lox* and higher collagen maturity were observed in coadministration studies, we investigated whether unimolecular dual GIP/GLP-2 analogues could recapitulate these findings. Similar to the coadministration studies, a dose of 100 pM was used to estimate the potency of unimolecular dual

GIP/GLP-2 analogues in murine MC3T3-E1 cells. Interestingly, with the exception of GL-0002, GL-0003, and GL-0009, all other unimolecular dual GIP/GLP-2 analogues significantly increased *Lox* expression compared with vehicle-treated murine cultures (Fig. 2A). However, compared with GIP- or GLP-2-treated cultures, only GL-0001 and GL-0007 significantly improved the extent of *Lox* expression (23%–34%, $p < 0.001$). As a result, unimolecular dual GIP/GLP-2 analogues that showed positive effects on *Lox* expression resulted in higher collagen maturity in murine cultures (Fig. 2B). Of note, GL-0001 and GL-0007 were the only two dual molecules that significantly enhanced the extent of collagen cross-linking beyond the effects of GIP or GLP-2.

We next thought to decipher whether the action of unimolecular dual GIP/GLP-2 analogues was due to synergism at both

Table 1. Affinity and Potency of Unimolecular Dual GIP/GLP-2 Analogues

	Human GIPr			Human GLP-2r			
	IC$_{50}$ (nM)	FRET ratio	FRET ratio fold change vs. GIP	IC$_{50}$ (nM)	FRET ratio	FRET ratio fold change vs. GLP-2	Coagonism score
GIP$_{1-30}$	0.97 ± 0.29	**1.52 ± 0.23**	-	**1.90 ± 0.32**	1.16 ± 0.22	0.63	0.54 ± 0.18
GLP-2	**11.55 ± 1.14**	1.07 ± 0.07	0.70	0.19 ± 0.04	**1.82 ± 0.32**	-	0.66 ± 0.09
GL-0001	1.19 ± 0.53	**1.49 ± 0.14**	0.98	0.44 ± 0.12	**1.65 ± 0.26**	0.90	0.98 ± 0.38
GL-0002	2.78 ± 0.82	1.06 ± 0.01	0.70	**15.16 ± 3.00**	1.19 ± 0.14	0.65	0.17 ± 0.03
GL-0003	0.72 ± 0.15	1.22 ± 0.06	0.80	**22.86 ± 3.67**	1.01 ± 0.04	0.56	0.17 ± 0.01
GL-0004	37.85 ± 14.8	1.00 ± 0.03	0.66	0.07 ± 0.02	**1.59 ± 0.29**	0.87	0.53 ± 0.24
GL-0005	**0.14 ± 0.04**	1.22 ± 0.13	0.80	15.05 ± 4.93	1.19 ± 0.11	0.65	0.33 ± 0.08
GL-0006	**4.60 ± 1.25**	1.04 ± 0.06	0.68	**1.04 ± 0.20**	1.15 ± 0.06	0.63	0.15 ± 0.04
GL-0007	1.05 ± 0.41	**1.56 ± 0.16**	1.02	0.57 ± 0.17	**1.54 ± 0.11**	0.84	0.89 ± 0.21
GL-0008	0.91 ± 0.25	**1.36 ± 0.08**	0.89	14.74 ± 5.69	1.34 ± 0.09	0.73	0.54 ± 0.07
GL-0009	**13.05 ± 3.14**	1.01 ± 0.09	0.66	**53.01 ± 11.9**	1.00 ± 0.04	0.55	0.03 ± 0.03

Note: Binding to the receptor was investigated in competition with FAM-GIP$_{1-30}$ or FAM-GLP-2 at the human GIPr and the human GLP-2r, respectively. Intracellular levels of cAMP were determined by ratiometric FRET using the H74 Epac-based FRET biosensor. The FRET ratio was investigated at the IC$_{50}$ concentration for all molecules (GIP$_{1-30}$, GLP-2, and dual analogues). The FRET ratio was standardized as 1 in the presence of vehicle only. Augmentation in the FRET ratio indicates increasing intracellular concentration of cAMP. FRET ratio fold change was computed as FRET ratio of dual analogue divided by FRET ratio of endogenous ligand. Coagonism was calculated as $\frac{(\text{FRET ratio (ligand)}-1)_{\text{GIPr}}+(\text{FRET ratio (ligand)}-1)_{\text{GLP2r}}}{(\text{FRET ratio(GIP)}-1)_{\text{GIPr}}+(\text{FRET ratio(GLP-2)}-1)_{\text{GLP2r}}}$. All experiments were carried in duplicate. IC$_{50}$ and FRET ratio are represented as mean ± SEM of three independent experiments. Bold value represents $p < 0.05$ vs. endogenous ligand.
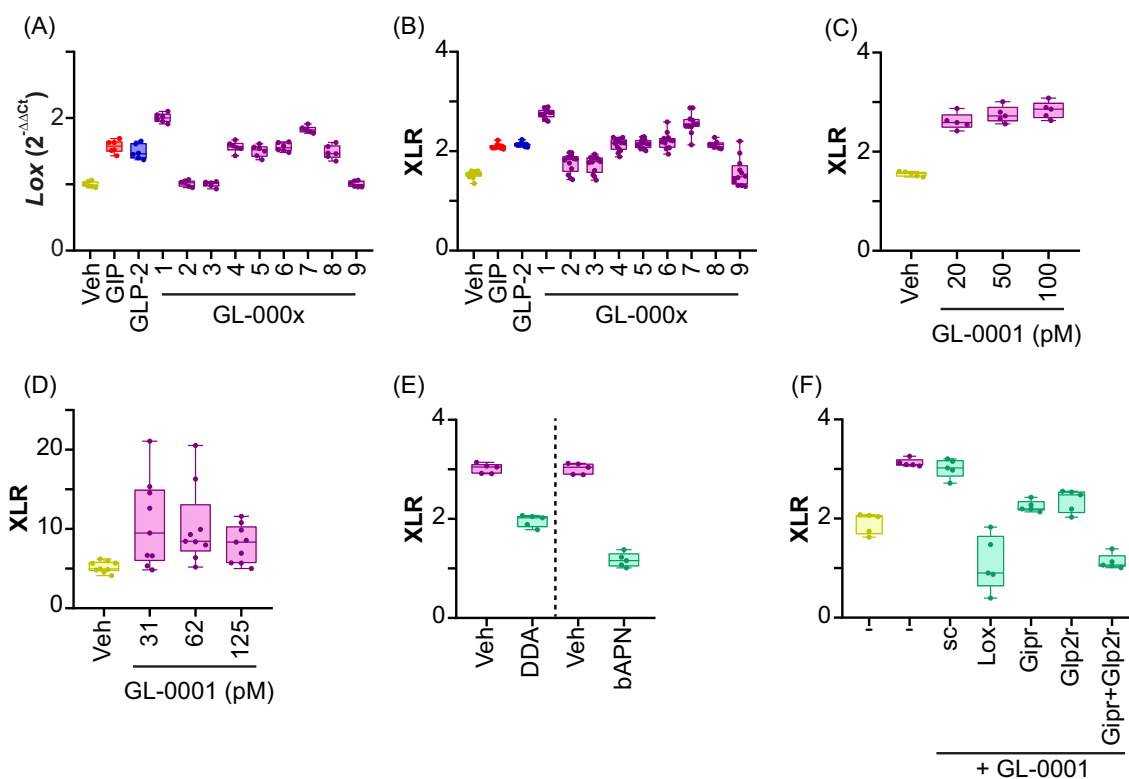
Fig. 2. Effects of newly designed unimolecular dual GIP/GLP-2 analogues on *Lox* expression and collagen maturity. (*A, B*) Murine MC3T3-E1 osteoblasts were treated with vehicle, 100 pM [D-Ala^2]GIP$_{1-30}$, 100 pM [Gly^2]GLP-2, or 100 pM of unimolecular dual GIP/GLP-2 analogues. *Lox* expression and collagen maturity (XLR) were determined after 14 days of treatment with the aforementioned peptides. (*C*) Murine MC3T3-E1 osteoblasts were treated with either vehicle or several concentrations (20–100 pM) of GL-0001 prior to collagen maturity evaluation. (*D*) Human primary osteoblast cells were cultured in the presence of several concentrations (31–125 pM) of GL-0001 prior to collagen maturity evaluation. (*E*) MC3T3-E1 cells were treated with either DDA or bAPN in the presence of 100 pM GL-0001 prior to collagen maturity evaluation. (*F*) MC3T3-E1 cells were incubated with 100 pM GL-0001 and siRNA targeting *Lox*, *Gipr*, *Glp2r*, both receptors (*Gipr+Glp2r*), or a scrambled siRNA (sc). Control cells were treated in the absence of siRNA (−). Statistical analyses are provided in Tables S2–S4. Data are presented as boxplot showing 25th and 75th percentiles, with whiskers, showing minimal and maximal values.

the GIPr and GLP-2r. In our case, it was not possible to perform the conventional isobologram analysis approach because GIP/GLP-2 coagonism is due to a sing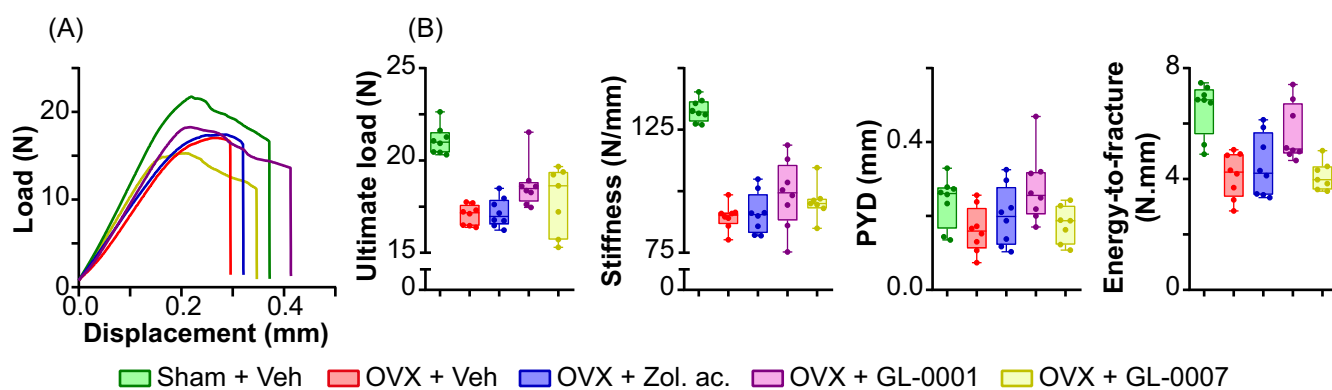le molecule, not a combination of two or more molecules. However, we computed the combination index according to Chou and Talalay,[39] assuming a bliss independence model. Effects on collagen maturity in murine cultures were used for combination index determination. Interestingly, GL-0001 and GL-0007 exhibited a combination index of 0.46 ± 0.07 and 0.65 ± 0.07, respectively, suggesting that both molecules possessed synergism properties (Table S5). GL-0005, GL-0006, and GL-0008 presented with a combination index suggesting additive effects. On the other hand, GL-0002, GL-0003, GL-0004, and GL-0009 presented with a combination index indicative of moderate to very strong antagonism.

In addition, improvement of collagen maturity in murine cultures observed with GL-0001 was not restricted to a dose of 100 pM but was already achieved at a lower dose of 20 pM (Fig. 2C). Recent reports suggested that activities at the murine and human receptors were not identical at the level of pancreatic islet, and this finding needed to be extended to bone receptors.[50] As such, we set out to assess whether the positive action of GL-0001 was restricted to rodents or whether it could be transferable to a human context. We treated primary human osteoblast cultures with ascending doses of GL-0001 in a range of 31–125 pM (Fig. 2D). GL-0001 significantly enhanced the extent of collagen cross-linking with maximum effects already encountered at 31 pM, suggesting that GL-0001 was also capable of activating rodent and human receptors.

We next tried to decipher whether the observed effects on collagen maturity was due to the activation of the cAMP-Lox pathways as seen for coadministration. Murine osteoblast cultures were repeated in the presence of the selective adenylyl cyclase inhibitor 2′, 5′-DDA. Here again, the effects of GL-0001 were blocked by pretreatment with this pharmacological inhibitor, suggesting that GL-0001 required a functional adenylyl cyclase to exert its effects (Fig. 2E). Similarly, pretreatment with bAPN significantly blocked the action of GL-0001 on collagen maturity, supporting the involvement of lysyl oxidase in this process. Furthermore, the use of specific siRNA targeting Lox, Gipr, Glp2r, or both receptors resulted in lower collagen maturity compared with the absence of siRNA, suggesting that these three genes are required for GL-0001 effects on collagen maturity (Fig. 2F).

Introduction of Gly² demonstrated resistance to dipeptidyl peptidase-4 degradation

We next verified whether the presence of a glycine residue at position 2 conferred resistance to DPP-4 as expected. PYY_{1-36} was used as a positive control. As reported in Fig. S4, for PYY_{1-36}, DPP-4 degradation was represented by the occurrence of the PYY_{3-36} fragment peptide, consistent with previous studies.[51] For GL-0001, the 3–33 fragment occurred only at 8 hours, suggesting that Gly² confers resistance to DPP-4. Indeed, the resistance half-life of GL-0001 was estimated at ~20 hours compared with ~8.5 minutes for PYY_{1-36}. However, as GL-0001$_{1-33}$

Fig. 3. Administration of GL-0001 improved bone biomechanical response in OVX mice. OVX mice were administered with vehicle, 25 nmoles/kg/day GL-0001, 25 nmoles/kg/day GL-0007, or once iv 100 μg/kg zoledronic acid. (A) Representative load–displacement curves obtained after 8 weeks of treatment and (B) biomechanical parameters including ultimate load, stiffness, postyield displacement (PYD), and energy-to-fracture. Statistical analyses were performed with one-way ANOVA with Dunnett's post hoc test. Data are presented as boxplot showing 25th and 75th percentiles, with whiskers, showing minimal and maximal values.

	ANOVA		Dunnett's multiple comparison						
			OVX+veh vs.				OVX+ZA vs.		
	F-value	p-value	Sham veh	OVX ZA	OVX GL1	OVX GL7	Sham veh	OVX GL1	OVX GL7
Ultimate load	17.92	<0.001	<0.001	0.998	0.021	0.420	<0.001	0.036	0.562
Stiffness	34.54	<0.001	<0.001	0.991	0.124	0.448	<0.001	0.237	0.672
PYD	3.193	0.025	0.129	0.689	0.013	0.984	0.660	0.142	0.931
Energy-to-fracture	10.66	<0.001	<0.001	0.880	0.008	>0.999	<0.001	0.0491	0.868

could be degraded, we next ascertained whether GL-0001$_{3-33}$ was potent in modulating collagen maturity in vitro. Interestingly, the cleaved form of GL-0001 did not induce a change in the collagen maturity response compared with vehicle and as opposed to the intact form. More importantly, when both forms, intact and cleaved, were coadded in the cultures, it did not reduce the extent of collagen maturity compared with the intact form only.

First-in-class unimolecular dual GIP/GLP-2 analogue GL-0001 improved bone strength and bone microstructure in OVX-induced bone fragility

We decided to further evaluate the benefit of the unimolecular dual GIP/GLP-2 analogue in the OVX-induced bone fragility model with zoledronic acid as a positive comparator. The efficiency of OVX has been assessed postmortem by uterus mass (Fig. S5). None of the pharmacological interventions influenced either body weight or blood glucose levels (Fig. S5). We investigated the biomechanical resistance of long bones following

saline or treatment administration. Interestingly, in the load–deformation curves, one notices that deformation is reduced in vehicle-treated OVX mice, suggesting that macroscopical fracture occurs rapidly after the coalescence of microcracks (Fig. 3A). This feature is not ameliorated by zoledronic acid administration. However, administration of GL-0001 or GL-0007 restored the pattern. Interestingly, GL-0001, but neither GL-0007 nor zoledronic acid, significantly improved ultimate load by 9% ($p = 0.021$), postyield deformation by 70% ($p = 0.013$), and energy-to-fracture by 37% ($p = 0.008$) (Fig. 3B). More importantly, the effects on ultimate load and energy-to-fracture were significantly different compared with zoledronic acid.

We next investigated whether improvement in the biomechanical response of bone following GL-0001 administration was due to changes in microstructure. As shown in Fig. 4A–C, vehicle-treated OVX animals presented with a similar cortical thickness and an 11% augmentation in tissue mineral density at the midshaft femuras compared with sham animals. None of the other microstructural parameters of cortical bone was significantly different (Fig. S6). At the tibia metaphysis (Fig. 4D–G), a
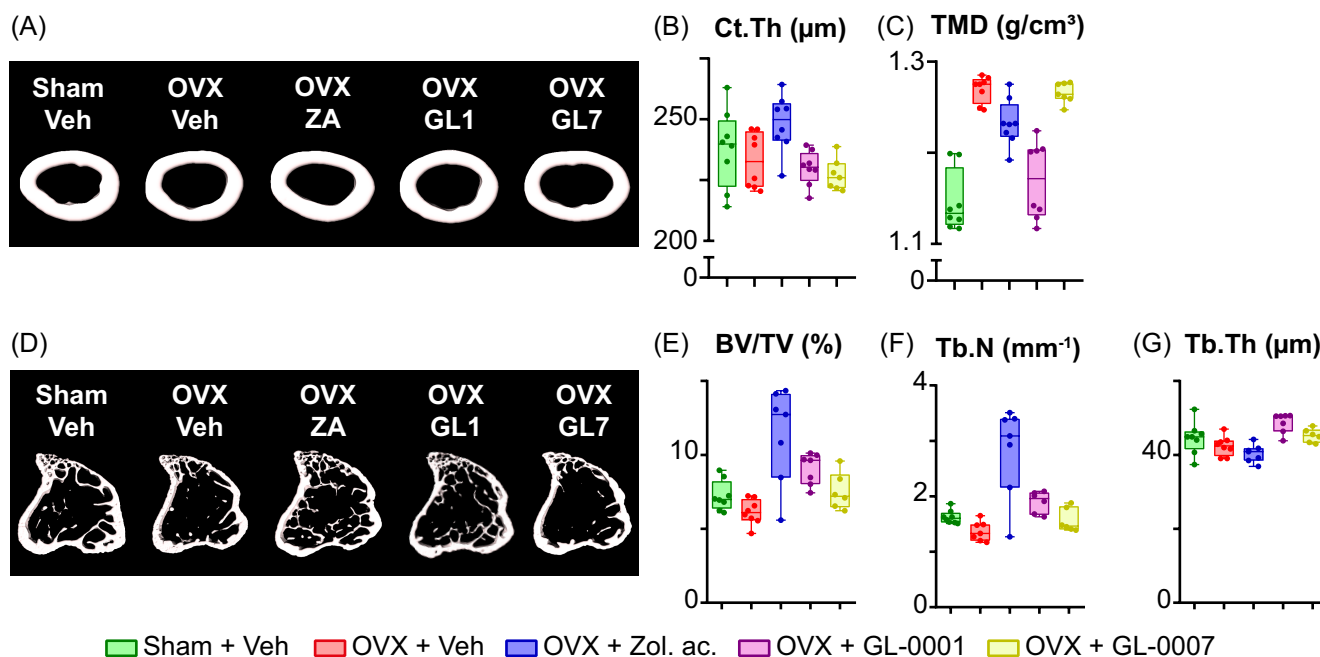
| | ANOVA | | Dunnett's multiple comparison | | | | | | |
| | | | OVX+veh vs. | | | | OVX+ZA vs. | | |
	F-value	p-value	Sham veh	OVX ZA	OVX GL1	OVX GL7	Sham veh	OVX GL1	OVX GL7
Ct.Th	4.22	0.007	0.815	0.037	0.947	0.698	0.214	0.009	0.003
TMD	31.12	<0.001	<0.001	0.042	<0.001	0.996	<0.001	<0.001	0.095
BV/TV	10.04	<0.001	0.523	<0.001	0.009	0.391	<0.001	0.062	0.001
Tb.N	13.84	<0.001	0.568	<0.001	0.086	0.795	<0.001	0.001	<0.001
Tb.Th	7.83	<0.001	0.413	0.525	0.001	0.260	0.037	<0.001	0.023

Fig. 4. Microstructural analyses of appendicular skeleton in OVX mice. (A) Representative 3D models, (B) cortical thickness, and (C) tissue mineral density (TMD) measured at femur midshaft. (D) Representative 3D models, (E) trabecular bone fraction, (F) no. trabeculae, and (G) trabecular thickness measured at tibia proximal metaphysis. Statistical analyses were performed with one-way ANOVA with Dunnett's post hoc test. Data are presented as box plot showing 25th and 75th percentiles, with whiskers, showing minimal and maximal values.

Fig. 5. Biochemical and histomorphometrical analyses of appendicular skeleton in OVX mice. (A) Circulating levels of parathyroid hormone (PTH). (B) Circulating levels of resorption marker CTX-I and (C, D) static osteoclast histomorphometry parameters. (E) Circulating levels of bone formation marker P1NP, (F) representative photographs of double labeling, and (G–I) dynamic histomorphometry parameters. Statistical analyses were performed with one-way ANOVA with Dunnett's post hoc test. Data are presented as boxplot showing 25th and 75th percentiles, with whiskers, showing minimal and maximal values.
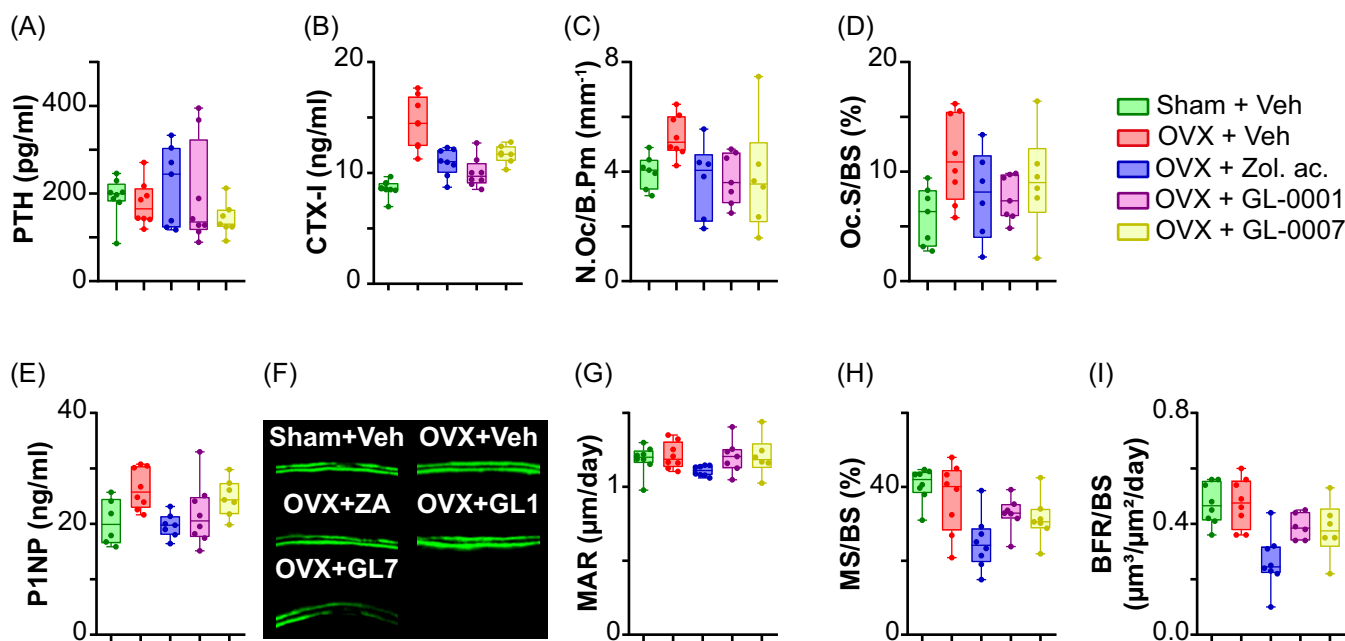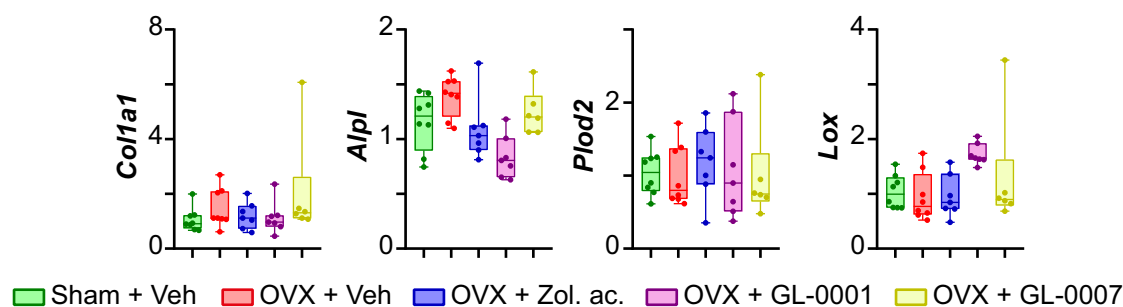
| | ANOVA | | Dunnett's multiple comparison | | | | | | |
| | | | OVX+veh vs. | | | | OVX+ZA vs. | | |
	F-value	p-value	Sham veh	OVX ZA	OVX GL1	OVX GL7	Sham veh	OVX GL1	OVX GL7
PTH	0.96	0.442							
CTX-I	17.74	<0.001	<0.001	<0.001	<0.001	<0.001	0.009	0.370	0.370
N.Oc/B.Pm	2.39	0.043	0.142	0.066	0.063	0.093	0.974	0.999	0.999
Oc.S/BS	2.33	0.046	0.025	0.256	0.173	0.647	0.722	0.999	0.923
P1NP	3.74	0.014	0.032	0.011	0.092	0.853	0.994	0.714	0.080
MAR	1.54	0.214							
MS/BS	6.22	<0.001	0.686	0.004	0.554	0.307	<0.001	0.102	0.225
BFR/BS	8.15	<0.001	>0.999	<0.001	0.225	0.151	<0.001	0.035	0.058

nonsignificant reduction in trabecular bone mass, due to a smaller number of trabeculae, was observed in vehicle-treated OVX. As expected, zoledronic acid administration significantly enhanced cortical thickness by 6% ($p = 0.037$) but also trabecular bone mass by 85% ($p < 0.001$) and trabeculae numbers by 106% ($p < 0.001$). Interestingly, GL-0001, but not GL-0007, significantly increased trabecular bone mass by 49% ($p = 0.009$) and trabecular thickness by 15% ($p = 0.001$) but had no significant effects on trabeculae numbers ($p = 0.086$) To further investigate whether the modifications of biomechanical response and trabecular microstructure were restricted to the appendicular skeleton, we also determined the biomechanical properties and trabecular microstructure at the fourth lumbar vertebral body. In the axial skeleton (Fig. S7), vehicle-treated OVX animals presented with significant reductions in ultimate load ($p = 0.005$), stiffness ($p = 0.002$), trabecular bone mass ($p = 0.009$), and trabecular number ($p = 0.021$). As expected, treatment with zoledronic acid led to a higher trabecular bone

mass and trabeculae number, which almost reached statistical significance ($p = 0.050$ and $p = 0.089$, respectively). However, zoledronic acid failed to significantly improve the biomechanical properties. On the other hand, neither GL-0001 nor GL-0007 improved significantly the biomechanical properties or trabecular microstructure at the axial skeleton. To better apprehend the cellular mechanism linked to observed changes in microstructure at the tibia, we evaluated the circulating levels of PTH$_{1-84}$, a key hormone in calcium and phosphate metabolism, and CTX-I and P1NP, two key molecules relevant to bone remodeling. No changes in circulating levels of PTH$_{1-84}$ were observed between the experimental groups (Fig. 5). As expected, circulating levels of the bone resorption marker CTX-I was significantly elevated by 41% ($p < 0.001$) in vehicle-treated OVX animals (Fig. 5). Interestingly, GL-0001-, GL-0007-, and zoledronic acid-treated OVX mice presented with significant reductions in this parameter of 31% ($p < 0.001$), 19% ($p < 0.001$), and 24% ($p < 0.001$), respectively (Fig. 5). At the cellular

Fig. 6. Expression levels of gene involved in posttranslational modifications of bone ECM. Statistical analyses were performed with one-way ANOVA with Dunnett's post hoc test. Data are presented as box plot showing 25th and 75th percentiles, with whiskers, showing minimal and maximal values.

level, the number of osteoclasts per bone perimeter and bone surfaces covered with osteoclasts showed similar patterns compared with CTX-I (Fig. 5). Zoledronic acid also led to a significant reduction in the circulating levels of the bone formation marker P1NP (-25%, $p = 0.011$), while no significant changes were observed with either GL-0001 or GL-0007 (Fig. 5). Dynamic bone histomorphometrical parameters suggested a reduction in active mineralizing surface and in bone formation rate with zoledronic acid but not with either GL-0001 or GL-0007 (Fig. 5).

Although GL-0001 was not designed to reduce osteoclast formation and/or resorption, the observed reduction in CTX-I levels and the apparent trend in lowering the number of osteoclasts and osteoclast surfaces led us to investigate whether coadministration of GIP and GLP-2 or GL-0001 had anti-osteoclastic properties. When single GIP and GLP-2 agonists were coadministered to murine osteoclast precursors cells, they significantly reduced the extent of osteoclast formation compared with vehicle or single agonists (Fig. S8A). GL-0001 administration in murine osteoclast precursors resulted in the same pattern (Fig. S8B). This effect was also seen in human osteoclast precursor cultures, where GL-0001 dose-dependently reduced osteoclast formation (Fig. S8C). More importantly, in human osteoclast cultures, GL-0001 dose-dependently reduced osteoclast resorption (Fig. S8D).

First-in-class unimolecular dual GIP/GLP-2 analogue GL-0001 improved bone ECM material properties in OVX-induced bone fragility

As unimolecular dual GIP/GLP-2 analogues have been developed to improve bone ECM material properties and do so in vitro, we thought to determine whether such effects were preserved in the OVX-induced bone fragility mouse model. As presented in Fig. 6, administration of either GL-0001 or GL-0007 did not modify either *Col1a1* or *Plod2* expression. However, GL-0001, but not GL-0007, significantly downregulated by 28% the expression of alkaline phosphatase ($p < 0.001$) and upregulated by 65% the

expression of *Lox* ($p = 0.028$). We next determined whether changes in *Alpl* and *Lox* expression, two key molecules involved in bone ECM maturation and mineralization, were related to modifications of bone ECM material properties. FTIR imaging highlighted changes in the mineral-to-matrix ratio and collagen maturity over the full cortical width (Fig. 7). Indeed, when quantified, the mineral-to-matrix ratio was significantly reduced by 2% ($p < 0.001$) in GL-0001-treated OVX mice compared with vehicle-treated OVX mice. Similarly, collagen maturity was enhanced in GL-0001-treated OVX mice by 10% ($p = 0.011$). None of these effects were observed with either zoledronic acid or GL-0007 (Fig. 7). Interestingly, the expression ratio of *Lox/Plod2* was significantly correlated with the extent of collagen maturity ($R^2 = 0.16$, F-value $= 5.88$, and $p = 0.021$). To further understand the contribution of mature and immature collagen cross-links to the observed change in collagen maturity, we monitored their spectral signature in the same bone sample (Fig. 7). We showed that mature cross-links and immature cross-links were increased by 3% ($p = 0.043$) and reduced by 8% ($p < 0.001$), respectively, suggesting an acceleration in the maturation of collagen postprocessing (Fig. 7). None of the other ECM material properties were altered in any of the studied groups.

Finally, to better understand whether changes at the microstructural and/or material levels were linked to the positive effects observed at the biomechanical level, we performed linear regression analyses between the CTX-I level, cortical thickness, collagen maturity, mineral-to-matrix ratio and energy-to-fracture. First, this analysis was conducted with all experimental groups included (Fig. 8A). CTX-I and collagen maturity were significantly associated with energy-to-fracture ($R^2 = 0.22$ and $p = 0.003$, and $R^2 = 0.27$ and $p < 0.001$, respectively). Because the mechanism of action of GL-0001 appeared different from that seen with zoledronic acid, we decided to redo these analyses by including only vehicle- and GL-0001-treated OVX animals (Fig. 8B). Interestingly, the CTX-I level ($R^2 = 0.16$, $p = 0.13$) was no longer significantly correlated with energy-to-fracture. However,
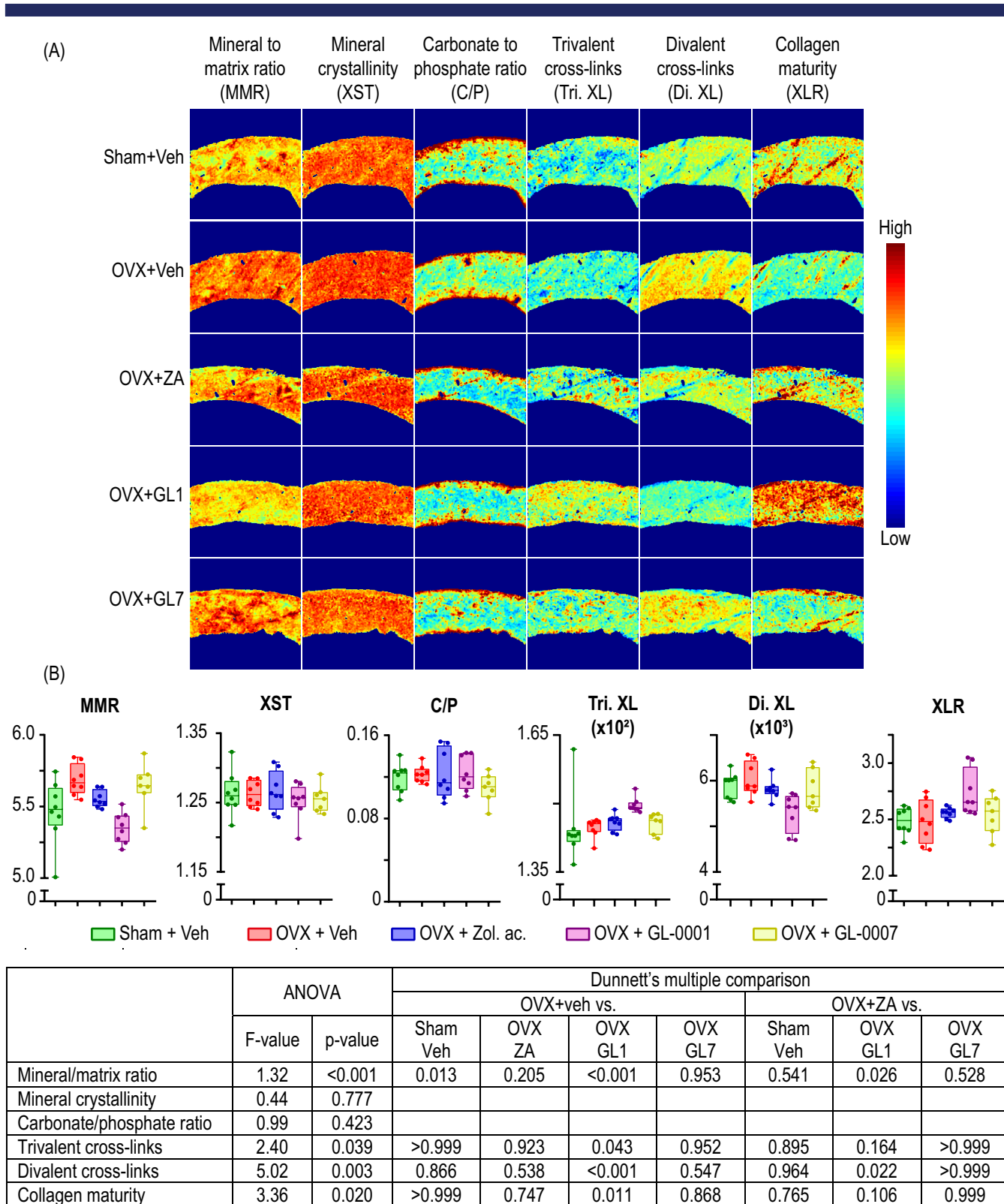
Fig. 7. GL-0001 ameliorated bone ECM material properties. (*A*) Representative imaging (FTIRI) images and (*B*) quantitative FTIRI parameters. Mineral-to-matrix ratio (MMR) represents the area ratio of the v1, v3 PO4/Amide I; mineral crystallinity/maturity (XST) was computed as the ratio between subpeaks localized at ~1030 and ~1020 cm^{-1}; carbonate-to-phosphate (C/P) ratio was computed as the ratio of the v3 carbonate and v1, v3 PO4; collagen maturity (XLR) was computed as the ratio between trivalent mature cross-link (Tri. XL)/divalent immature crosslink (Di. XL). Mature and immature cross-links were normalized by Amide I area. Statistical analyses were performed with one-way ANOVA with Dunnett's post hoc test. Data are presented as boxplot showing 25th and 75th percentiles, with whiskers, showing minimal and maximal values.

The table from the figure:

| | ANOVA | | Dunnett's multiple comparison | | | | | | |
| | | | OVX+veh vs. | | | | OVX+ZA vs. | | |
	F-value	p-value	Sham Veh	OVX ZA	OVX GL1	OVX GL7	Sham Veh	OVX GL1	OVX GL7
Mineral/matrix ratio	1.32	<0.001	0.013	0.205	<0.001	0.953	0.541	0.026	0.528
Mineral crystallinity	0.44	0.777							
Carbonate/phosphate ratio	0.99	0.423							
Trivalent cross-links	2.40	0.039	>0.999	0.923	0.043	0.952	0.895	0.164	>0.999
Divalent cross-links	5.02	0.003	0.866	0.538	<0.001	0.547	0.964	0.022	>0.999
Collagen maturity	3.36	0.020	>0.999	0.747	0.011	0.868	0.765	0.106	0.999

(A)

● Sham + Veh ● OVX + Veh ● OVX + Zol. ac. ● OVX + GL-0001 ● OVX + GL-0007

Energy-to-fracture vs.	Linear regression analysis (all groups)			
	R^2	F-value	p-value	Equation
CTX-I	0.216	9.933	0.003	Energy-to-fracture=-0.241*CTX-I+7.646
Ct.Th	0.026	0.978	0.329	Energy-to-fracture =-0.016*Ct.Th+8.822
XLR	0.273	13.90	<0.001	Energy-to-fracture =3.936*XLR-5.106
MMR	0.047	1.807	0.187	Energy-to-fracture =-1.245*MMR+11.89

(B)

● OVX + Veh ● OVX + GL-0001

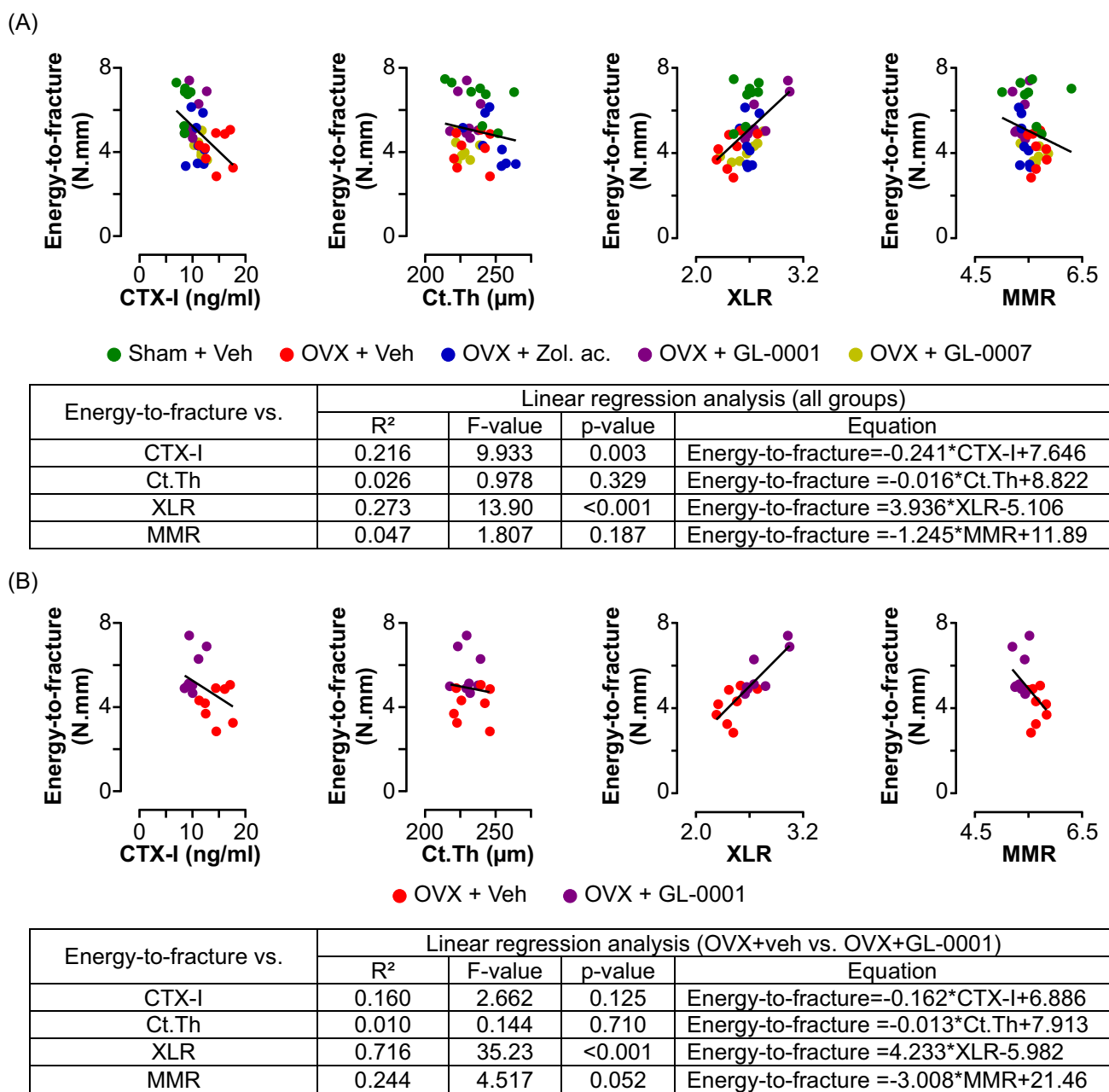| Energy-to-fracture vs.	Linear regression analysis (OVX+veh vs. OVX+GL-0001)			
	R^2	F-value	p-value	Equation
CTX-I	0.160	2.662	0.125	Energy-to-fracture=-0.162*CTX-I+6.886
Ct.Th	0.010	0.144	0.710	Energy-to-fracture =-0.013*Ct.Th+7.913
XLR	0.716	35.23	<0.001	Energy-to-fracture =4.233*XLR-5.982
MMR	0.244	4.517	0.052	Energy-to-fracture =-3.008*MMR+21.46

Fig. 8. Regression analyses between biomechanical, CTX-I levels, cortical thickness, and bone ECM material properties. Linear regressions were performed by either including all experimental groups (A) or only OVX + veh and OVX + GL-0001 groups (B). Linear regression analyses were performed; R^2, F-value, p-value, and equation are reported.

the amelioration of collagen maturity ($R^2 = 0.72$, $p < .001$) and possibly a lower mineral-to-matrix ratio ($R^2 = 0.24$, $p = 0.052$) seemed linked to the improvement in bone biomechanical resistance, suggesting that targeting bone ECM material properties with GL-0001 could enhance bone resistance to fracture.

Discussion

All current therapeutic approaches to reducing the burden of fragility fracture rely on increasing bone mineral density as a surrogate to enhance bone strength. In contrast, based on our previous work with single-parent peptides,[14-22] we conceived and reported herein the development of a first-in-class unimolecular dual GIP/GLP-2 analogue, GL-0001, establishing it as more efficacious than zoledronic acid in reducing bone fragility in an OVX mouse model of bone fragility. Through a series of chemical changes that yielded a hybrid peptide sequence, we identified GL-0001 as a high-potency balanced dual analogue capable of binding to and activating the GIPr and GLP-2r, resistant to DPP-4 degradation, that enhances collagen maturity in vitro in murine and human osteoblast cultures and improves bone strength, mostly by modulating bone ECM material properties in vivo.

Interestingly, GL-0001 also limited bone osteoclast resorption and ultimately led to the preservation of trabecular bone mass in the appendicular skeleton. Of note, we evidenced that GL-0001 was capable of reducing osteoclast formation but also osteoclast-mediated resorption in osteoclast cultures. Previously, a similar effect was encountered with single GIP analogues[52-54] or single GLP-2 analogues.[18,55] Furthermore, subcutaneous administration of GIP or GLP-2 or coadministration of GIP and GLP-2 in healthy individuals resulted in a marked decrease in CTX-I levels and was mirrored by an acute suppression of parathyroid hormone (PTH) secretion.[26,56] Both receptors appeared to be expressed with the same magnitude in parathyroid gland tissues, but only GLP-2, not GIP, demonstrated antiresorptive actions through reduced secretion of PTH.[25] Currently, the function of GIPr on the parathyroid gland remains to be fully elucidated. Interestingly, in our study, we failed to demonstrate any significant change in circulating PTH levels following GL-0001 administration, despite a clear reduction in CTX-I levels, ruling out any PTH-mediated effects to explain the antiresorptive properties of GL-0001. However, we clearly showed that GL-0001 reduced the number of newly generated osteoclasts in murine and in human cultures and reduced the extent of bone resorption, suggesting that the observed reduction in CTX-I levels was more likely due to direct effects on osteoclast precursors/mature osteoclasts. Nevertheless, recent evidence also suggests that joint administration of GIP and GLP-2 in postmenopausal subjects is more potent in reducing circulating levels of CTX-I compared with a single infusion of GIP or GLP-2.[57] Our data are in accordance with such mechanisms. Indeed, the administration of GL-0001 to cultured human osteoclast precursor elicited a significant reduction in osteoclast-mediated bone resorption and osteoclast precursor differentiation. This is also in agreement with the recent observation that GIPr and GLP-2r are expressed by human osteoclasts.[25] However, in our study, despite a significant reduction in CTX-I levels with GL-0007 treatment, no effects of this molecule were observed in modulating bone ECM material properties and enhancing bone mechanical resistance in vivo. Our regression study unambiguously showed that the improved biomechanical response of bone with GL-0001 was mostly due to changes in bone ECM material properties but not with either cortical thickness or CTX-I levels. Although it is tempting and practical to monitor the effects of unimolecular dual GIP/GLP-2 analogues with a simple blood test in humans, it is not a proof of efficacy in improving bone biomechanical response.

Unimolecular dual GIP/GLP-2 analogues were developed to bring to the therapeutic arsenal against bone fragility new molecules that could directly target bone ECM material properties. Single GIP or GLP-2 analogues were characterized previously, and several analogues exhibited significant effects on bone material properties by targeting *Lox* expression and/or post-translational modifications of bone collagen, including cross-linking and maturity.[14,18-23,58,59] During optimization of the consensus sequence, we noticed that amino acid positions 7, 10, 12, and 13 were crucial to balancing the activity of unimolecular GIP/GLP-2 analogues at GIPr or GLP-2r. An isoleucine at position 12 had been shown previously to be vital for selective GIP activity in a series of unimolecular dual GIP/GLP-1 agonists,[44] whereas substitution of Thr^{12} by Ala^{12} in GLP-2 reduced the generation of cAMP.[43] Interestingly, GL-0001 and GL-0007 revealed that dual agonism at hGIPr and hGLP-2r differed only at positions 10, 31, 32, and 33. The methionine residue at position 10 is the natural amino acid in human GLP-2. In contrast, at this position, human GIP exhibits a tyrosine residue. The use of Met^{10} in GL-0001 conserved activity at both hGIPr and hGLP-2r. The use of Phe^{10} in GL-0007, with similar side chain length compared with endogenous Tyr^{10}, also led to balanced activity at both receptors, at least in vitro. It is not clear now whether bias toward either the GIPr or GLP-2r, as seen for unimolecular dual GIP/GLP-1 compound tirzepatide,[60] could be beneficial in improving bone strength to a greater extent than seen with GL-0001. However, this should be further investigated in the future.

Recently, others have reported the development of another unimolecular dual GIP/GLP-2 analogue, peptide 11, that shows ~79% similarity with GL-0001.[56] However, and in opposition to GL-0001, peptide 11 demonstrated a species-dependency bias toward either GIPr or the GLP-2r in human and rodent systems, respectively. This behavior was not found with GL-0001 as a similar enhancement of collagen maturity was observed in human and rodent cultures. Furthermore, and to the best of our knowledge, no bone data have been reported for peptide 11, so it is not possible to compare the activity of GL-0001 to this other unimolecular dual GIP/GLP-2 analogue. Nevertheless, GL-0001 led to significant amelioration of biomechanical resistance to fracture and clearly reversed compromised bone ECM material properties in OVX animals.

In this study, we observed that vehicle-treated OVX animals exhibited higher tissue mineral density and mineral-to-matrix ratio, suggesting a higher degree of mineralization of the bone matrix. This observation had already been reported by others.[61,62] The molecular mechanism remains unclear, but it has been postulated that this modification represents a mechanoregulatory response to bone loss and an adaptative compensatory response triggered by the loss of neighboring bone, whereby the remaining bone undergoes a compensatory shift in mineral content to counteract the loss of structural strength. Whether this adaptation requires changes in the composition of the organic part of the bone matrix (reduction in collagen content, changes in noncollagenous protein) remains to be investigated. It is plausible that the effect of GL-0001 on tissue mineral density is due to a change in the deposition of noncollagenous protein that can modulate the deposition of bone mineral. This matter needs to be investigated in the future.

It should be noted, however, that a number of assumptions and limitations are associated with this study that require some discussion. First, this study was performed in a mouse model of OVX-induced bone loss. This model, although useful, does not present all the characteristics of osteoporotic bone observed in humans.[63] Second, recently, Sparre-Ulrich and coworkers reported differences between rodent and human receptors in response to GIP analogues in the pancreas.[50] Whether such discrepancy also occurs in bone tissue remains to be investigated, and despite the clear evidence presented in this article that GL-0001 exhibited a similar response in mouse and human bone cells in vitro, this is not a guarantee of similar activity in vivo. A study performed in a small group of osteoporotic humans will be a prerequisite to further assess the utility of dual GIP/GLP-2 analogues in the treatment of bone fragility. Third, we did not investigate tissue modulus and hardness by nanoindentation or equivalent methods, despite clear modification in several tissue material properties. In particular, the molecular mechanisms leading to a reduced mineral-to-matrix ratio require further investigation.

In conclusion, we developed a series of unimolecular dual GIP/GLP-2 analogues with the first-in-class molecule, GL-0001,

capable of enhancing collagen maturity and directly improving bone biomechanical response and resistance to fracture in vivo. GL-0001, and more broadly unimolecular dual GIP/GLP-2 analogues, represents a new therapeutic solution for the treatment and prevention of bone fragility that targets bone material properties rather than bone mineral density. This innovative pathway represents an interesting and complementary enhancement to the conventional therapeutic arsenal in the treatment of patients suffering from bone fragility.

Acknowledgments

Disclosure

GM is an inventor with a patent pending on unimolecular dual GIP/GLP-2 analogues for the treatment of bone disorders.

Author Contributions

Benoit Gobron: Investigation; formal analysis; writing – original draft. **Malory Couchot:** Investigation; formal analysis; writing – review & editing. **Nigel Irwin:** Investigation; formal analysis; writing – review & editing. **Erick Legrand:** Conceptualization; resources; writing – review & editing. **Béatrice Bouvard:** Conceptualization; resources; supervision; writing – review & editing. **Guillaume Mabilleau:** Conceptualization; investigation; writing – review & editing; formal analysis; supervision; funding acquisition; data curation.

Peer Review

The peer review history for this article is available at https://publons.com/publon/10.1002/jbmr.4792.

Data Availability Statement

The data that support the findings of this study are available from the corresponding author upon reasonable request.

References

1. Oden A, McCloskey EV, Kanis JA, Harvey NC, Johansson H. Burden of high fracture probability worldwide: secular increases 2010-2040. Osteoporos Int. 2015;26(9):2243–2248.

2. Marx D, Rahimnejad Yazdi A, Papini M, Towler M. A review of the latest insights into the mechanism of action of strontium in bone. Bone Rep. 2020;12:100273.

3. Cosman F, Crittenden DB, Adachi JD, et al. Romosozumab treatment in postmenopausal women with osteoporosis. N Engl J Med. 2016; 375(16):1532–1543.

4. Cummings SR, San Martin J, McClung MR, et al. Denosumab for prevention of fractures in postmenopausal women with osteoporosis. N Engl J Med. 2009;361(8):756–765.

5. Black DM, Delmas PD, Eastell R, et al. Once-yearly zoledronic acid for treatment of postmenopausal osteoporosis. N Engl J Med. 2007; 356(18):1809–1822.

6. Kanis JA, Norton N, Harvey NC, et al. SCOPE 2021: a new scorecard for osteoporosis in Europe. Arch Osteoporosis. 2021;16(1):82.

7. Alliston T, Schafer A. Bone quality sleuths: uncovering tissue-level mechanisms of bone fragility in human type 2 diabetes. J Bone Miner Res. 2019;34(7):1189–1190.

8. Torres-del-Pliego E, Vilaplana L, Guerri-Fernandez R, Diez-Perez A. Measuring bone quality. Curr Rheumatol Rep. 2013;15(11):373.

9. Gaar J, Naffa R, Brimble M. Enzymatic and non-enzymatic crosslinks found in collagen and elastin and their chemical synthesis. Org Chem Front. 2020;7:2789–2814.

10. Alliston T. Biological regulation of bone quality. Curr Osteoporos Rep. 2014;12(3):366–375.

11. Chen K, Zhao J, Qiu M, et al. Osteocytic HIF-1alpha pathway manipulates bone micro-structure and remodeling via regulating osteocyte terminal differentiation. Front Cell Dev Biol. 2021;9:721561.

12. Dole NS, Mazur CM, Acevedo C, et al. Osteocyte-intrinsic TGF-beta signaling regulates bone quality through Perilacunar/Canalicular remodeling. Cell Rep. 2017;21(9):2585–2596.

13. Shi C, Mandair GS, Zhang H, et al. Bone morphogenetic protein signaling through ACVR1 and BMPR1A negatively regulates bone mass along with alterations in bone composition. J Struct Biol. 2018;201(3): 237–246.

14. Gobron B, Bouvard B, Vyavahare S, et al. Enteroendocrine K cells exert complementary effects to control bone quality and mass in mice. J Bone Miner Res. 2020;35(7):1363–1374.

15. Mieczkowska A, Bouvard B, Chappard D, Mabilleau G. Glucose-dependent insulinotropic polypeptide (GIP) directly affects collagen fibril diameter and collagen cross-linking in osteoblast cultures. Bone. 2015;74:29–36.

16. Mieczkowska A, Bouvard B, Legrand E, Mabilleau G. [Gly(2)]-GLP-2, but not glucagon or [D-ala(2)]-GLP-1, controls collagen crosslinking in murine osteoblast cultures. Front Endocrinol. 2021;12:721506.

17. Mieczkowska A, Irwin N, Flatt PR, Chappard D, Mabilleau G. Glucose-dependent insulinotropic polypeptide (GIP) receptor deletion leads to reduced bone strength and quality. Bone. 2013;56(2):337–342.

18. Gobron B, Bouvard B, Legrand E, Chappard D, Mabilleau G. GLP-2 administration in ovariectomized mice enhances collagen maturity but did not improve bone strength. Bone Rep. 2020;12:100251.

19. Vyavahare SS, Mieczkowska A, Flatt PR, Chappard D, Irwin N, Mabilleau G. GIP analogues augment bone strength by modulating bone composition in diet-induced obesity in mice. Peptides. 2020; 125:170207.

20. Mansur SA, Mieczkowska A, Flatt PR, et al. A new stable GIP-Oxyntomodulin hybrid peptide improved bone strength both at the organ and tissue levels in genetically-inherited type 2 diabetes mellitus. Bone. 2016;87:102–113.

21. Mansur SA, Mieczkowska A, Bouvard B, et al. Stable Incretin Mimetics counter rapid deterioration of bone quality in type 1 diabetes mellitus. J Cell Physiol. 2015;230(12):3009–3018.

22. Mabilleau G, Mieczkowska A, Irwin N, et al. Beneficial effects of a N-terminally modified GIP agonist on tissue-level bone material properties. Bone. 2014;63:61–68.

23. Mabilleau G, Gobron B, Mieczkowska A, Perrot R, Chappard D. Efficacy of targeting bone-specific GIP receptor in ovariectomy-induced bone loss. J Endocrinol. 2018;239(2):215–227.

24. Hansen MS, Søe K, Christensen LL, Fernandez-Guerra P, Hansen NW, Wyatt RA, et al. GIP receptor reduces osteoclast activity and improves osteoblast survival by activating multiple signaling pathways. 2022: 498420.

25. Skov-Jeppesen K, Hepp N, Oeke J, et al. The antiresorptive effect of GIP, but not GLP-2, is preserved in patients with hypoparathyroidism-a randomized crossover study. J Bone Miner Res. 2021;36(8):1448–1458.

26. Skov-Jeppesen K, Svane MS, Martinussen C, et al. GLP-2 and GIP exert separate effects on bone turnover: a randomized, placebo-controlled, crossover study in healthy young men. Bone. 2019;125: 178–185.

27. Canelon SP, Wallace JM. Beta-Aminopropionitrile-induced reduction in enzymatic crosslinking causes In vitro changes in collagen morphology and molecular composition. PLoS One. 2016;11(11): e0166392.

28. Klarenbeek JB, Goedhart J, Hink MA, Gadella TW, Jalink K. A mTurquoise-based cAMP sensor for both FLIM and ratiometric read-out has improved dynamic range. PLoS One. 2011;6(4):e19170.

29. Mabilleau G, Petrova NL, Edmonds ME, Sabokbar A. Increased osteoclastic activity in acute Charcot's osteoarthropathy: the role of receptor activator of nuclear factor-kappaB ligand. Diabetologia. 2008; 51(6):1035–1040.

30. Mabilleau G, Sabokbar A. Interleukin-32 promotes osteoclast differentiation but not osteoclast activation. PLoS One. 2009;4(1):e4173.

31. Bouxsein ML, Boyd SK, Christiansen BA, Guldberg RE, Jepsen KJ, Muller R. Guidelines for assessment of bone microstructure in rodents using micro-computed tomography. J Bone Miner Res. 2010;25(7):1468–1486.

32. Chappard D, Alexandre C, Riffat G. Histochemical identification of osteoclasts. Review of current methods and reappraisal of a simple procedure for routine diagnosis on undecalcified human iliac bone biopsies. Basic Appl Histochem. 1983;27(2):75–85.

33. van't Hof RJ, Rose L, Bassonga E, Daroszewska A. Open source software for semi-automated histomorphometry of bone resorption and formation parameters. Bone. 2017;99:69–79.

34. Dempster DW, Compston JE, Drezner MK, et al. Standardized nomenclature, symbols, and units for bone histomorphometry: a 2012 update of the report of the ASBMR Histomorphometry nomenclature committee. J Bone Miner Res. 2013;28(1):2–17.

35. Ammann P, Badoud I, Barraud S, Dayer R, Rizzoli R. Strontium ranelate treatment improves trabecular and cortical intrinsic bone tissue quality, a determinant of bone strength. J Bone Miner Res. 2007;22(9):1419–1425.

36. Jepsen KJ, Silva MJ, Vashishth D, Guo XE, van der Meulen MC. Establishing biomechanical mechanisms in mouse models: practical guidelines for systematically evaluating phenotypic changes in the diaphyses of long bones. J Bone Miner Res. 2015;30(6):951–966.

37. Turner CH, Burr DB. Basic biomechanical measurements of bone: a tutorial. Bone. 1993;14(4):595–608.

38. Aguado E, Mabilleau G, Goyenvalle E, Chappard D. Hypodynamia alters bone quality and trabecular microarchitecture. Calcif Tissue Int. 2017;100(4):332–340.

39. Chou TC, Talalay P. Quantitative analysis of dose-effect relationships: the combined effects of multiple drugs or enzyme inhibitors. Adv Enzyme Regul. 1984;22:27–55.

40. Paschalis EP, Verdelis K, Doty SB, Boskey AL, Mendelsohn R, Yamauchi M. Spectroscopic characterization of collagen cross-links in bone. J Bone Miner Res. 2001;16(10):1821–1828.

41. Hansen LS, Sparre-Ulrich AH, Christensen M, et al. N-terminally and C-terminally truncated forms of glucose-dependent insulinotropic polypeptide are high-affinity competitive antagonists of the human GIP receptor. Br J Pharmacol. 2016;173(5):826–838.

42. Wisniewski K, Sueiras-Diaz J, Jiang G, et al. Synthesis and pharmacological characterization of novel glucagon-like peptide-2 (GLP-2) analogues with low systemic clearance. J Med Chem. 2016;59(7): 3129–3139.

43. DaCambra MP, Yusta B, Sumner-Smith M, Crivici A, Drucker DJ, Brubaker PL. Structural determinants for activity of glucagon-like peptide-2. Biochemistry. 2000;39(30):8888–8894.

44. Finan B, Ma T, Ottaway N, et al. Unimolecular dual incretins maximize metabolic benefits in rodents, monkeys, and humans. Sci Transl Med. 2013;5(209):209ra151.

45. Yaqub T, Tikhonova IG, Lattig J, et al. Identification of determinants of glucose-dependent insulinotropic polypeptide receptor that interact with N-terminal biologically active region of the natural ligand. Mol Pharmacol. 2010;77(4):547–558.

46. Parthier C, Kleinschmidt M, Neumann P, et al. Crystal structure of the incretin-bound extracellular domain of a G protein-coupled receptor. Proc Natl Acad Sci U S A. 2007;104(35):13942–13947.

47. Zhao F, Zhang C, Zhou Q, et al. Structural insights into hormone recognition by the human glucose-dependent insulinotropic polypeptide receptor. eLife. 2021;10:e68719.

48. Sun W, Chen LN, Zhou Q, et al. A unique hormonal recognition feature of the human glucagon-like peptide-2 receptor. Cell Res. 2020; 30(12):1098–1108.

49. Drucker DJ, Shi Q, Crivici A, et al. Regulation of the biological activity of glucagon-like peptide 2 in vivo by dipeptidyl peptidase IV. Nat Biotechnol. 1997;15(7):673–677.

50. Sparre-Ulrich AH, Hansen LS, Svendsen B, et al. Species-specific action of (Pro3)GIP—a full agonist at human GIP receptors, but a partial agonist and competitive antagonist at rat and mouse GIP receptors. Br J Pharmacol. 2016;173(1):27–38.

51. Lafferty RA, Gault VA, Flatt PR, Irwin N. Effects of 2 novel PYY(1-36) analogues, (P(3)L(31)P(34))PYY(1-36) and PYY(1-36)(Lys(12)PAL), on pancreatic Beta-cell function, growth, and survival. Clin Med Insights Endocrinol Diabetes. 2019;12:1179551419855626.

52. Mabilleau G, Perrot R, Mieczkowska A, et al. Glucose-dependent insulinotropic polypeptide (GIP) dose-dependently reduces osteoclast differentiation and resorption. Bone. 2016;91:102–112.

53. Tsukiyama K, Yamada Y, Yamada C, et al. Gastric inhibitory polypeptide as an endogenous factor promoting new bone formation after food ingestion. Mol Endocrinol. 2006;20(7):1644–1651.

54. Zhong Q, Itokawa T, Sridhar S, et al. Effects of glucose-dependent insulinotropic peptide on osteoclast function. Am J Physiol Endocrinol Metab. 2007;292(2):E543–E548.

55. Lu Y, Lu D, Hu Y. Glucagon-like peptide 2 decreases osteoclasts by stimulating apoptosis dependent on nitric oxide synthase. Cell Prolif. 2018;51(4):e12443.

56. Gabe MBN, Skov-Jeppesen K, Gasbjerg LS, et al. GIP and GLP-2 together improve bone turnover in humans supporting GIPR-GLP-2R co-agonists as future osteoporosis treatment. Pharmacol Res. 2022;176:106058.

57. Skov-Jeppesen K, Veedfald S, Madsbad S, Holst JJ, Rosenkilde MM, Hartmann B. Subcutaneous GIP and GLP-2 inhibit nightly bone resorption in postmenopausal women: a preliminary study. Bone. 2021;152:116065.

58. Daley EJ, Pajevic PD, Roy S, Trackman PC. Impaired gastric hormone regulation of osteoblasts and Lysyl oxidase drives bone disease in diabetes mellitus. JBMR Plus. 2019;3(10):e10212.

59. Daley EJ, Trackman PC. Beta-catenin mediates glucose-dependent insulinotropic polypeptide increases in lysyl oxidase expression in osteoblasts. Bone Rep. 2021;14:101063.

60. Willard FS, Douros JD, Gabe MB, et al. Tirzepatide is an imbalanced and biased dual GIP and GLP-1 receptor agonist. JCI Insight. 2020; 5(17):e140532.

61. Boyde A, Compston JE, Reeve J, et al. Effect of estrogen suppression on the mineralization density of iliac crest biopsies in young women as assessed by backscattered electron imaging. Bone. 1998;22(3): 241–250.

62. McNamara LM, Ederveen AG, Lyons CG, et al. Strength of cancellous bone trabecular tissue from normal, ovariectomized and drug-treated rats over the course of ageing. Bone. 2006;39(2): 392–400.

63. Jilka RL. The relevance of mouse models for investigating age-related bone loss in humans. J Gerontol, Ser A. 2013;68(10):1209–1217.